Peer-reviewed version available at *Biomolecules* **2019**, *9*, 371; doi:10.3390/biom9080371

Structural Changes in the Acceptor Site of Photosystem II Upon Ca^{2+}/Sr^{2+} Exchange in the Mn_4CaO_5 Cluster Site and the Possible Long-Range Interactions

Faisal Hammad Mekky Koua,*[1,2]

[1]*Center for Free Electron Laser Science, Deutsches Elektronen-Synchrotron (DESY), Notkestrasse 85, Hamburg 22607, Germany*
[2]*National University Biomedical Research Institute, National University-Sudan, Air St. PO Box 3783, Khartoum, Sudan*

*Correspondence information:

Center for Free Electron Laser Science, DESY, Notkestr. 85, Hamburg 22607, Germany. Email: faisal.koua@cfel.de

Abstract

Structural perturbations in the Mn_4CaO_5 cluster site, an oxygen-evolving complex of photosystem II, such as those induced by Ca^{2+}/Sr^{2+} exchanges or Ca/Mn-removal have been known to induce long-range positive shifts (+30 mV to +150 mV) in the redox potential of the primary quinone electron acceptor plastoquinone A (QA) located 40 Å distant from the OEC. Here, we reanalyzed the crystal structure of Sr-PSII solved at 2.1 Å and compare it with the native Ca-PSII of 1.9 Å with focus on the acceptor site and report on the possible long-range interactions between the donor, $Mn_4Ca(Sr)O_5$ cluster, and acceptor sites.

Keywords: photosystem II; redox potential; electron transfer; charge separation; photo-inhibition

Main text

Photosystem II (PSII) is a large multi-subunit membrane protein complex with at least 19 subunits and exists physiologically as a dimer of ca. 0.70 MDa molecular weight embedded in the thylakoid membranes of oxygenic photosynthetic organisms [1]. PSII catalyzes one of the most fundamental reactions on Earth that is the light-induced charge separation and water oxidation [1-3]. PSII initiates the photosynthetic reactions by absorbing light via its internal antenna pigments leading to a charge-separation of the reaction center chlorophyll pigments, so called P680, a process that leads to a release of an electron and formation of $P680^{\bullet+}$ and $Pheo^{\bullet-}$ ionic radicals [4-6]. Then, the released electron serves to reduce the plastoquinone in Q_A site ($Q_A/Q_A^{\bullet-}$), a redox couple that reduces a mobile Q_B with two consecutive electrons in the Q_B site leading to the formation of plastoquinol (Q_BH_2) by taking up two protons from the stroma. Q_BH_2 then detaches from the Q_B site and moves

Preprints (www.preprints.org) | NOT PEER-REVIEWED | Posted: 27 June 2019 doi:10.20944/preprints201906.0278.v1

Peer-reviewed version available at Biomolecules 2019, 9, 371; doi:10.3390/biom9080371

into the plastoquinol pool in the membrane spanning region [6]. The highly reactive $P680^{\bullet+}/Pheo^{\bullet-}$ and subsequent secondary radical pairs formed due to charge separation could be stabilized by oxidizing the catalytic center Mn_4CaO_5 cluster, also called the donor site, via a redox active tyrosine (D1-Tyr161). The P680 has the highest redox potential known in biology, E_m =1.3 V (vs. SHE), which enables it to subtract electrons from and fully oxidizes two water molecules by accumulating oxidizing equivalents consecutively in the Mn_4CaO_5 cluster during Sn-state transitions, where n = 0-4 [5,6].

The high-resolution XRD structures of PSII provided a detailed picture on the architecture of the protein matrix and the co-factors arrangements involved in the light-induced plastoquinone-reduction and water oxidation processes (Fig. 1) [2,3]. However, the mechanistic basis of these processes still not fully understood. Of which, for instance, the role of Ca^{2+} in PSII light-induced water oxidation. Ca^{2+} has long been known as an essential element for water oxidation [3-7]. For example, Ca^{2+} removal was found to suppress the formation of higher-oxidation states beyond S_2 state [7]. This effect can be retrieved by Ca^{2+} or partially (ca. 40-50%) by Sr^{2+} reconstitution into Ca^{2+} depleted PSII [3,7-9]. This implies that there is a supervening rearrangement on the donor site of PSII, and likely in other locations within the electron transfer (ET) chain. Indeed, fluorescence imaging data on Sr-modified OEC PSII crystals showed altered properties of functional PSII, i.e. slowdown in the ET from Q_A to Q_B and a stabilized $S_2Q_A^-$ charge recombination [10]. Consistent with this, a modified ET kinetics on the donor site accompanied with conformational changes on the acceptor site was observed upon perturbations in the donor sites by Ca^{2+}/Sr^{2+} (not by Cl^-/Br^-) exchanges and that this exchange upshifted the redox potential (E_m) of Q_A^-/Q_A by ~+30 mV [6,11]. Moreover, even a larger upshift in the E_m (Q_A/Q_A^-) with ~+150 mV and relatively smaller shift (E_m = +20 mV) in the non-heme iron (NHI) was reported previously in Mn-depleted PSII, which is likely affecting the Ca^{2+} binding to the OEC [4]. These results indicate that the ET events between the donor and acceptor sites are highly tuned and governed not only by the redox brokers along the ET pathway but also by the protein moiety as well as the conformational changes within the OEC vicinity. The mechanism behind the effects of these perturbations in the Mn_4CaO_5 cluster on the electrochemical properties of Q_A-Fe^{2+}-Q_B and what are the structural changes that take place on the acceptor site in response to such perturbations remain largely unclear. Note that the Mn_4CaO_5 cluster is far distant (~40Å) from the acceptor site (Fig. 1) [2,3].

Preprints (www.preprints.org) | NOT PEER-REVIEWED | Posted: 27 June 2019 doi:10.20944/preprints201906.0278.v1

Peer-reviewed version available at Biomolecules 2019, 9, 371; doi:10.3390/biom9080371

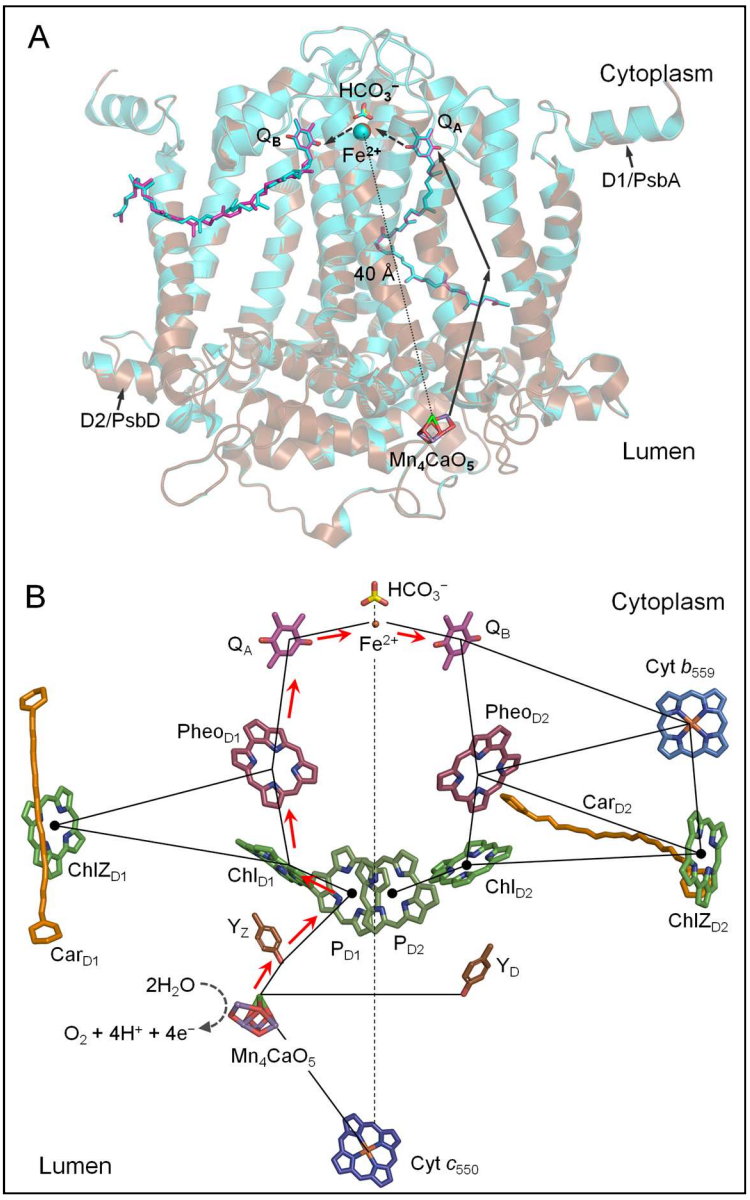

Figure 1. Electron transport pathway in photosystem II complex. (A) Superimposed structures of the D1/D2 proteins from native (cyan; PDB: 3WU2) and Sr-modified OEC (brown; PDB: 4IL6) photosystem II. The figure highlights the donor (Mn_4CaO_5 cluster) and the acceptor (Q_A-Fe^{2+}/HCO_3^--Q_B) sites, which are in about 40 Å apart. (B) The ET pathway and the locations of main cofactors involved in the electron transfer process.

In our previous report on the Sr^{2+}-PSII structure at 2.1 Å, we focused on the conformational changes that occurred in the $Mn_4Ca(Sr)O_5$ cluster and its local environment [3]. To further investigate the possible effects of Ca^{2+}/Sr^{2+} exchange in the long-range interactions with the acceptor site, the structure of Sr-PSII (PDB: 4IL6) [3] was revisited in comparison with the native Ca-PSII model of 1.9Å resolution (PDB: 3WU2) [2] with main focus on the primary quinone electron acceptor (QA) site as well as the local environment of the acceptor site Q_A-Fe^{2+}-Q_B (Fig. 1). It was reported previously that OEC perturbations by Ca^{2+}/Sr^{2+} exchange induces slight differences localized mainly in the OEC and nearby H-bonding networks mediated by water molecules. Significant change was observed at the

Preprints (www.preprints.org) | NOT PEER-REVIEWED | Posted: 27 June 2019 doi:10.20944/preprints201906.0278.v1

Peer-reviewed version available at Biomolecules 2019, 9, 371; doi:10.3390/biom9080371

position of W3 – a water molecule binds to the Ca^{2+}/Sr^{2+}, which might be responsible from the O_2 evolution reduction by ~60% comparing to the native PSII [2,3,12]. This is reasonable since the incorporation of Sr^{2+} takes place in the OEC site and such conformational changes are expected to reduce the activity [3].

Figure 2 shows the structural comparison between Ca-PSII and Sr-PSII at the local vicinity of the BCT-Fe^{2+}-His(4) and nearby Q_A and Q_B sites. Q_A is located between the primary electron acceptor and the NHI site and mediates ET in PSII reactions (Fig. 1) [2]. It is thus reasonable to attribute the redox potential shifts of Q_A to the structural changes upon Mn/Ca depletion or Ca^{2+}/Sr^{2+} exchanges [5,10,11,13]. Q_A is stabilized by van der Waals interactions including two moderate H-bonds via its carbonyl oxygens (C=O1, proximal and C=O2, distal) to N-Phe261-D2 and N_δ-His214-D2, respectively, as well as a π-stacking interaction with a nearby highly conserved D2-Trp253 (Table 1; Fig. 3) [2,14]. This interaction is similar to the corresponding native Q_A interaction with slightly higher thermal motion, i.e. 10-20% increase in the temperature (B) factors (Table 1). This similarity indicates that the midpoint redox potential shifts (~+30 mV) observed upon Ca^{2+}/Sr^{2+} exchange could likely be due to indirect effects or due to other H-bonding mediators or electrostatic forces. Recent attenuated total reflection (ATR) FTIR difference spectroscopy study excluded the direct influence of Mn_4CaO_5 cluster perturbations on the Q_A site [5]. The D2-Thr217 was previously predicted to form an additional H-bond with the C=O (proximal) of Q_A and thus contributes to the positive shifts observed in the $E_m(Q_A^-/Q_A)$ [12]. We observed that this residue forms a moderate H-bond with the indole nitrogen ($N_\varepsilon 1$) of nearby D2-Trp253 (~2.8 Å), whereas it interacts weakly (weak electrostatic) with the proximal C=O of Q_A with a shorter H-bond (~ –0.2 Å) in the Sr-PSII model implying a formation of H-bond in Sr-PSII, but not in Ca-PSII (~ 3.9 Å) (Fig. 3A,B). These differences are similar between the two monomers of each model, although it roughly lies within the r.m.s.d value (0.21 Å) of the Cα atoms of Sr-PSII and Ca-PSII [2,3]. Such differences may give rise to different electrostatic energies between mediators and thus shifting their redox potentials [15,16]. Note that in the case of Ca^{2+}/Sr^{2+} exchange, the E_m (Q_A) shift is only ~ +30 mV comparing to +150 mV when Ca^{2+} or Mn(s) are depleted [4,5]. By comparing the H-bonding with that of the Mn-depleted structure (PDB: 5MX2), we observed even shorter bond distance (3.48 Å) between the proximal C=O with the D2-Thr217 indicating an additional H-bond formation upon Mn-depletion [17]. This is in agreement with theoretical prediction and might be a cause for the upshifts in the E_m of Q_A [13]. Similar behavior was also observed in the H-bonding environment of the primary quinone acceptor of the bacterial reaction center (bRC) [18-20]. The D2-Thr217 and D2-Trp253 are highly conserved between the bRC and PSII, thus similar mechanism is highly expected [2,21]. Interestingly, the structural changes upon Ca^{2+}/Sr^{2+} exchanges or Mn-depletion gave rise to weaker H-bonds between the proximal C=O of Q_A with the imidazole nitrogen (N_δ) of D2-His214 with average distances of 2.79(+0.13) Å and 2.95(+0.29) Å, respectively [2,3,17]. The additional D2-Thr217 H-bond to Q_A results into a similar H-bonding environment between Q_A and Q_B (Fig. 3A,B), which might be a cause for the decrease in the redox potential gap

Preprints (www.preprints.org) | NOT PEER-REVIEWED | Posted: 27 June 2019 doi:10.20944/preprints201906.0278.v1

Peer-reviewed version available at Biomolecules 2019, 9, 371; doi:10.3390/biom9080371

(ΔE_m) and hence causes an impairment in the forward ET while enhancing a direct charge recombination with P680 [22]. The perturbations in the His-Q_A interaction may affect their electrostatic coupling and perturbs the E_m of Q_A. Moreover, the increased stabilization of Q_A with an additional H-bond from D2-Thr217 could lead to the positive shift in the redox potential [13]. It should be noted that such positive shifts might vary depending on the H-bond strength and hence the stability of Q_A. Therefore, the weak H-bond between D2-Thr217 and the C=O1 of Q_A in the Sr-PSII model might be the reason for the relatively smaller shifts, 30% lower than the E_m upshifts of the Ca/Mn removal [5,6].

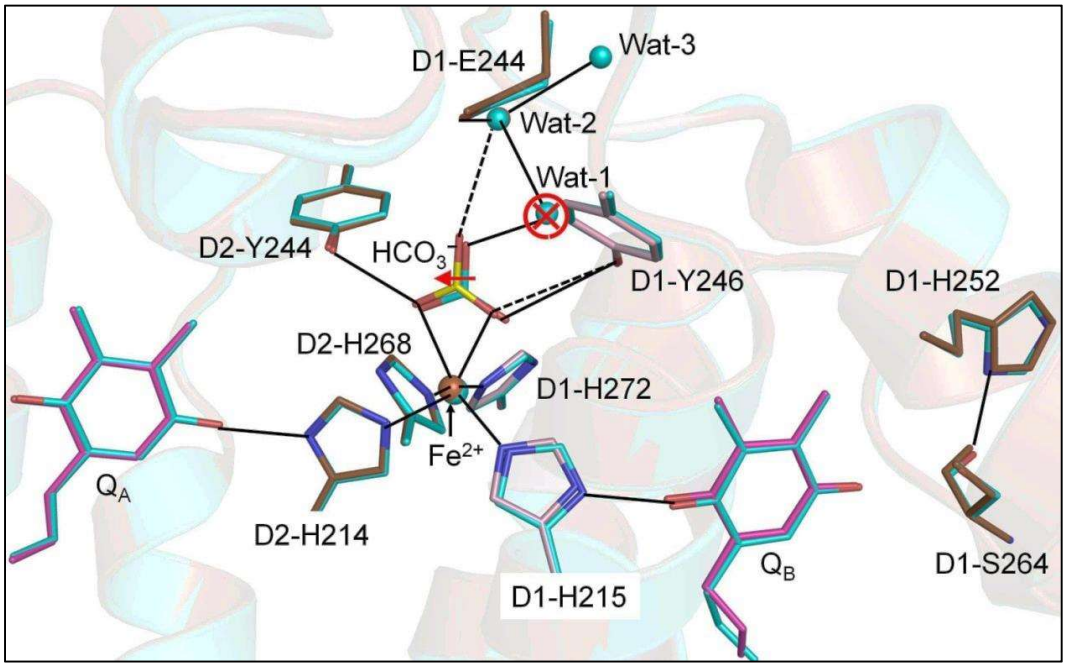

Figure 2. Superimposition of native Ca-PSII (PDB: 3WU2) and Sr-PSII (PDB: 4IL6) at the acceptor site pocket. The solid and dashed-lines indicate the hydrogen-bonding network within the acceptor site possibly facilitate the ET/PT pathways that include two Q_A, Q_B, bicarbonate, NHI, and water molecules. The red arrow and open-circle indicate the major differences between native Ca-PSII and Sr-PSII.

Preprints (www.preprints.org) | NOT PEER-REVIEWED | Posted: 27 June 2019 doi:10.20944/preprints201906.0278.v1

Peer-reviewed version available at Biomolecules 2019, 9, 371; doi:10.3390/biom9080371

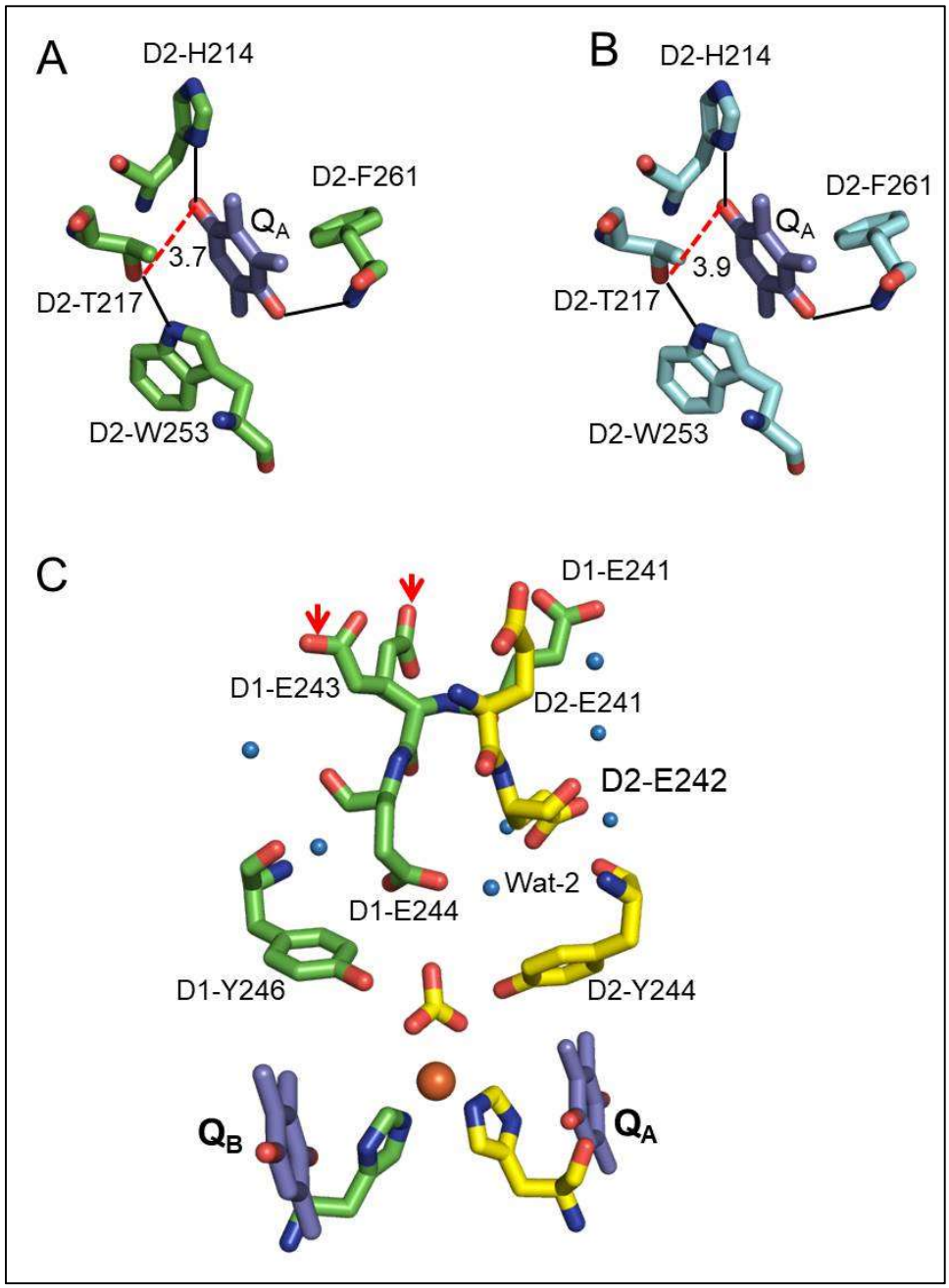

Figure 3. The immediate environment of Q_A and its relations to the distant stromal Glu residues. A) The interactions of Q_A with nearby residues and the additional H-bond (red dashed-line) with D2-T217, B) the correspondent environment of Q_A in the Ca-PSII model. C) The distant stromal Glu residues and associated water molecules. The red arrows indicate the rotamers of D1-E243 residue in Sr-PSII model.

Preprints (www.preprints.org) | NOT PEER-REVIEWED | Posted: 27 June 2019 doi:10.20944/preprints201906.0278.v1

Peer-reviewed version available at Biomolecules 2019, 9, 371; doi:10.3390/biom9080371

Table 1 The average interatomic distances of the acceptor site of Sr-PSII (PDB: 4IL6) and native Ca-PSII (PDB: 3WU2) and their corresponding temperature B-factors.

Ligand	Subunit	Sr-PSII / Å	Ca-PSII / Å	B-factor	Sr-PSII / Å^2	Ca-PSII / Å^2
Fe(II)				Fe(II)	29.61(0.42)	27.41(0.52)
NE2-His215	psbA/D1	2.06(0.02)	2.16(0.03)	NE2-His215	28.48(0.17)	25.75(0.79)
NE2-His214	psbD/D2	2.10(0.01)	2.17(0.07)	NE2-His214	27.24(1.97)	23.72(0.20)
NE2-His268	psbD/D2	2.20(0.02)	2.28(0.02)	NE2-His268	27.22(1.31)	24.37(0.30)
NE2-His272	psbA/D1	2.26(0.04)	2.26(0.01)	NE2-His272	29.67(0.94)	28.25(0.26)
O1-BCT	psbD/D2	2.30(0.02)	2.33(0.00)	O1-BCT	39.41(0.77)	31.23(0.24)
O2-BCT	psbD/D2	2.39(0.02)	2.29(0.05)	O2-BCT	39.74(0.68)	34.04(0.23)
Quinone B				O1/Q_B	52.37(0.55)	60.45(0.20)
O1/ND1-His215	psbA/D1	2.50(0.00)	2.48(0.06)	O2/Q_B	52.73(0.53)	74.23(0.19)
O2/OG-Ser264	psbA/D1	2.76(0.06)	2.74(0.02)	OG-Ser264	48.57(0.46)	63.62(0.17)
O2/N-Phe265	psbA/D1	2.82(0.09)	2.95(0.05)	N-Phe265	47.07(0.51)	57.01(0.19)
O2/O2-Phe265	psbA/D1	3.15(0.19)	3.09(0.08)	O2-Phe265	49.90(0.49)	66.33(0.18)
				ND1-His215	30.16(1.94)	27.23(0.16)
Quinone A				O2/Q_A	28.47(0.58)	25.13(0.21)
O2/ND1-His214	psbD/D2	2.79(0.00)	2.66(0.06)	O1/Q_A	28.60(0.62)	25.60(0.22)
O1/N-Phe261	psbD/D2	3.02(0.00)	2.95(0.03)	ND1-His214	27.32(0.47)	22.80(0.44)
				N-Phe261	26.74(0.45)	23.36(0.17)

Note: Values presented here are averages of two monomers and the data between parentheses are the standard deviations between two monomers.

We next analysed the structural differences between Sr-PSII and Ca-PSII at the NHI site (Fig. 2). The NHI does not involve in the ET process between Q_A and Q_B. It binds to four histidine residues, of which two residues, the D2-His214 and D1-His215, form direct H-bonds with the proximal C=O of Q_A and Q_B, respectively. Several differences were observed in the NHI site between the two models, for example, significant displacement was observed in the NHI of monomer A (0.42 Å). The BCT, which binds the NHI with a bidentate via two C=O groups, is also displaced significantly in the Sr-PSII model with an average of 0.37 Å in the two monomers (Fig. 2). This displacement has led to significant changes in the H-bonding network within the immediate environment of the NHI. In the Ca-PSII model, the BCT is in H-bonding distances with the phenol hydroxyls of D1-Tyr246 and D2-Tyr244 with 3.33 Å and 2.99 Å, respectively. These H-bond distances were significantly elongated in the Sr-PSII model especially the H-bond to the D1-Tyr246, which elongated by +0.31Å (3.64 Å). The role of BCT in PSII is controversial [23], however, a recent report has shown that it involves in the redox tuning of PSII perhaps by modulating its binding strength during the ET [24]. This might explain the perturbed interactions of BCT to the NHI (Table 1) and D1-Tyr246 upon Ca^{2+}/Sr^{2+} exchange and likely the positive shift in the E_m of Q_A.

Preprints (www.preprints.org) | NOT PEER-REVIEWED | Posted: 27 June 2019 doi:10.20944/preprints201906.0278.v1

Peer-reviewed version available at Biomolecules 2019, 9, 371; doi:10.3390/biom9080371

Recently, Kato *et al*. (2016) using an FTIR difference spectroscopy have reported that the positive shifts in the mid-point redox potential of Q_A^-/Q_A might be due to a modulation in the pK_a of distant carboxylate residues in the stromal site of PSII [5]. There are indeed 5 Glu residues, D1-Glu242, D1-Glu243, D1-Glu244, D2-Glu241 and D2-Glu242 in ~15 Å from the NHI center and 55 Å away from the Mn_4CaO_5 cluster toward the stromal side (Fig. 3A,B) [2,3]. Together, these residues form intensive H-bonding networks involving several water molecules from the stromal site to the NHI center (Fig. 3C). Two significant structural changes between Sr-PSII and Ca-PSII exist in this region. First, the H-bonding between BCT C=O and two water molecules, denoted wat-1 and wat-2, is broken due to a loss of wat-1 in the Sr-PSII model (Fig. 2). Wat-1 functions as a bridge between the BCT and these Glu residues via intensive H-bonding network beginning from wat-2 and D1-Glu244 and so up to the D1-Glu242 on the stromal site. In the Sr-PSII model the D1-Glu244 forms a weak H-bond with one of the C=O of BCT in the absence of wat-1 (Fig. 2). Wat-1 also mediates the interaction between the BCT and D1-Ser268 residues which binds the D1-His272, a ligand of the NHI [2,3]. However, it is not clear whether the absence of this water molecule can cause such a shift in the redox potential of Q_A site or not. Interestingly, wat-1 is preserved in the Mn-depleted structure in a single monomer, whereas both water molecules are absent in the second monomer [17]. The second difference was observed in one of the Sr-PSII monomer, where the side chain of D1-Glu243 residue formed two prominent rotamers with 0.5 occupancy for each monomer (Fig. 3C). Such rotameric conformational changes indicate the dynamic nature of D1-Glu243 and hence its involvement in the electrostatic interaction with the acceptor site. It is important to note that the similarity between the two monomers of PSII are still debated, hence such differences between the two monomers cannot be excluded [25]. Further theoretical studies are required to justify the effects of the modulation of the electrostatic interactions of these Glu residues on the redox potential of Q_A and their long-range interactions with the Mn_4CaO_5 cluster.

Conclusion

In summary, the present work highlights the structural changes that take place in the acceptor site of PSII upon perturbations in the Mn_4CaO_5 cluster due to Ca^{2+}/Sr^{2+} exchanges. We show that several structural changes have occurred at three different levels upon Ca^{2+}/Sr^{2+} exchanges; i) the additional H-bonding at the Q_A site formed by D2-Thr217, ii) the perturbations of BCT interactions with the NHI and nearby Tyr residues, and iii) the differences in the H-bonding network formed by the distal Glu residues at the stromal side with the NHI binding site. Some of these structural changes might be responsible from the positive shifts of the mid-point redox potential of the primary quinone electron acceptor Q_A and hence impairs the forward ET and enhance the backward ET and direct charge recombination between the Q_A and the $P680^+$, which is important for preventing PSII from the photo-inhibition.

Acknowledgments

I would like to thank Drs. Shen J-R and Umena Yasufumi for their assistance in the Sr-PSII project at Okayama University. I would like to acknowledge the financial support from the European Research Council ERC grant (no. 609920).

References

[1] Shen, J.-R. The structure of photosystem II and the mechanism of water oxidation in photosynthesis. *Ann. Rev. Plant Biol.* **2015**, *66*, 23–48.

[2] Umena, Y.; Kawakami, K.; Shen, J.-R.; Kamiya, N. Crystal structure of oxygen-evolving photosystem II at a resolution of 1.9 Å. *Nature*, **2011**, *473*, 55–60.

[3] Koua, F.H.M.; Umena, Y.; Kawakami, K.; Shen, J.-R. Structure of Sr-substituted photosystem II at 2.1 A resolution and its implications in the mechanism of water oxidation. *Proc. Natl. Acad. Sci. U.S.A.* **2013**, *110*, 3889–3894.

[4] Kato, Y.; Noguchi, T. Long-Range Interaction between the Mn4CaO5 Cluster and the Non-heme Iron Center in Photosystem II as Revealed by FTIR Spectroelectrochemistry. *Biochemistry*, **2014**, *53*, 4914–4923.

[5] Kato, Y.; Ishii, R.; Noguchi, T. Comparative analysis of the interaction of the primary quinone QA in intact and Mn-depleted photosystem II membranes using light-induced ATR-FTIR spectroscopy. *Biochemistry*, **2016**, *55*, 6355–6358.

[6] Kato, Y.; Shibamoto, T.; Yamamoto, S.; Watanabi, T.; Ishida, N.; Sugiura, M.; Rappaport, F.; Boussac, A. Influence of the PsbA1/PsbA3, Ca^{2+}/Sr^{2+} and Cl^{-}/Br^{-} exchanges on the redox potential of the primary quinone Q_A in Photosystem II from *Thermosynechococcus elongatus* as revealed by spectroelectrochemistry. *Biochim. Biophys. Acta Bionenerg*. **2012**, *1817*, 1998–2004.

[7] Boussac, A.; Rappaport, F.; Carrier, P.; Verbavatz, J.M.; Gobin, R.; Kirilovsky, A.; Rutherford, A.W.; Sugiura, M. Biosynthetic Ca^{2+}/Sr^{2+} Exchange in the Photosystem II Oxygen-evolving Enzyme of *Thermosynechococcus elongatus*. *J. Biol. Chem.*, **2004**, *279*, 22809–22819.

[8] Boussac, A.; Sugiura, M.; Rappaport, F. Probing the quinone binding site of photosystem II from *Thermosynechococcus elongatus* containing either PsbA1 or PsbA3 as the D1 protein through the binding characteristics of herbicides. *Biochim. Biophys. Acta Bioenerg.* **2011**, *1807*, 119–129.

[9] Krieger, A.; Rutherford, A.W.; Johnson, G.N. On the determination of redox midpoint potential of the primary quinone electron acceptor, QA, in photosystem II. *Biochim. Biophys. Acta Bioenerg*. **1995**, *1229*, 193–201.

[10] Kargul, J.; Maghlaoui, K.; Murray, J.W.; Deak, Z.; Boussac, A.; Rutherford, A.W.; Vass, I.; Barber, J. Purification, crystallization and X-ray diffraction analyses of the *T. elongatus* PSII core dimer with strontium replacing calcium in the oxygen-evolving complex. *Biochim. Biophys. Acta Bioenerg*. **2007**, *1767*, 404–413.

[11] Saito, K.; Rutherford, A.W.; Ishikita, H. Mechanism of proton-coupled quinone reduction in photosystem II. *Proc. Natl. Acad. Sci. U.S.A.* **2013**, *110*, 954–959.

[12] Chatterjee, R.; Milikisiyants, S.; Coates, C.S.; Koua, F.H.M.; Shen, J.R.; Lakshmi, K.V. The structure and activation of substrate water molecules in Sr2+-substituted photosystem II. *Phys. Chem. Chem. Phys.* **2014**, *16*, 20834–20843.

[13] Ishikita, H.; Knapp, E.W. Control of quinone redox potentials in photosystem II: Electron transfer and photoprotection. *J. Am. Chem. Soc.* **2005**, *127*, 14714–14720.

[14] Chen, J.; Chen, J.; Liu, Y.; Zheng, Y.; Zhu, Q.; Han, G.; Shen, J.-R. Proton-coupled electron transfer of plastoquinone redox reactions in photosystem II: a pump-probe ultraviolet resonance Raman study. *J. Phys. Chem. Lett.* **2019**, *10*, 3240–3247.

[14] Moore, G.R.; Pettigrew, G.W.; Rogers, N.K. Factors influencing redox potentials of electron transfer proteins. *Proc. Natl. Acad. Sci. U.S.A.* **1986**, *83*, 4998–4999.

[15] Zhou, H.X.; Pang, X. Electrostatic interactions in protein structure, folding, binding, and condensation. *Chem. Rev.* **2018**, *118*, 1691-1741.

[16] M. Zhang, M.; Bommer, M.; Chatterjee, R.; Husseon, R.; Yano, J.; Dau, H.; Kern, J.; Dobbek, H.; Zouni, A. Structural insights into the light-driven auto-assembly process of the water-oxidizing Mn_4CaO_5-cluster in photosystem II. *eLife* **2017**, *6*:e2693.

[17] Breton, J.; Boullais, C.; Burie, J.R.; Nabedryk, E.; Mioskowski, C. Binding sites of quinones in photosynthetic bacterial reaction centers investigated by light-induced FTIR difference spectroscopy: Symmetry of the carbonyl interactions and close equivalence of the QB vibrations in *Rhodobacter sphaeroides* and *Rhodopseudomonas viridis* probed by isotope labelling. *Biochemistry* **1994**, *33*, 14378–14386.

[18] Brudler, R.; de Groot, H.J.M.; van Liemt, W.B.S.; Steggerda, W.F.; Esmeijer, R.; Gast, P.; Hoff, A.J.; Lugtenburg, J.; Gerwert, K. Asymmetric binding of the 1- and 4-C=O groups of QA in *Rhodobacter sphaeroides* R26 reaction centers monitored by Fourier transform infra-red spectroscopy using site-specific isotopically labelled ubiquinone-10. *EMBO J* **1994**, *13*, 5523–5530.

[19] Zhu, Z.; Gunner, M.R. Energetics of quinone-dependent electron and proton transfers in *Rhodobacter sphaeroides* reaction centres. *Biochemistry* **2005**, *44*, 82–96.

[20] Ermler, U.; Fritzsch, G.; Buchanan, S.K.; Michel, H. Structure of the photosynthetic reaction center from *Rhodopbacter sphaeroides* at 2.65 Å resolution: cofactors and protein-cofactor interactions. *Structure* **1994**, *2*, 935–936.

[21] Ashizawa, R.; Noguchi, T. Effects of hydrogen bonding interactions on the redox potential and molecular vibrations of plastoquinone as studied using density functional theory calculations. *Phys. Chem. Chem. Phys.* **2014**, *16*, 11864–11876.

[22] Shevela, D.; Eaton-Rye, J.J.; Shen, J.-R.; Govindjee. Photosystem II and the unique role of bicarbonate: a historical perspective. *Biochim. Biophs. Acta Bioenerg*. **2012**, *1817*, 1134–1151.

[23] Brinkert, K.; De Causmaecker, S.; Kriger-Liszkay, A.; Fantuzzi, A.; Rutherford, A.W. Bicarbonate-induced redox tuning in photosystem II for regulation and protection. *Proc. Natl. Acad. Sci. USA* **2016**, *113*, 1244–12149.

[24] A. Tanaka, A.; Fukushima, Y.; Kamiya, N. Two different structures of the oxygen-evolving complex in the same polypeptide frameworks of photosystem II. *J. Am. Chem. Soc.* **2017**, *139*, 1718–1721.